The Redshift Evolution of Clustering in the HDF

M.Magliocchetti¹, S.J.Maddox^{1,2}

- ¹ Institute of Astronomy, Madingley Road, Cambridge CB3 0HA
- ²School of Physics and Astronomy, University of Nottingham, Nottingham, NG7 2RD, UK.

7 June 2021

ABSTRACT

We present a correlation function analysis for the catalogue of photometric redshifts obtained from the Hubble Deep Field image by Fernandez-Soto et al., 1998. By dividing the catalogue into redshift bins of width $\Delta z = 0.4$ we measured the angular correlation function $w(\theta)$ as a function of redshift up to $z \sim 4.8$. From these measurements we derive the trend of the correlation length r_0 . We find that $r_0(z)$ is roughly constant with look-back time up to $z \simeq 2$, and then increases to higher values at $z \gtrsim 2.4$. We estimate the values of r_0 , assuming $\xi(r,z) = (r/r_0(z))^{-\gamma}$, $\gamma = 1.8$ and different geometries. For $\Omega_0 = 1$ we find $r_0(z = 3) \simeq 7.00 \pm 4.87 \ h^{-1}$ Mpc, in good agreement with the values obtained from analysis of the Lyman Break Galaxies.

Key words: galaxies: clustering - galaxies: general - cosmology: observations - large-scale structure

1 INTRODUCTION

The evolution of galaxy clustering provides vital clues to the formation of galaxies and large-scale structure. The amplitude of galaxy clustering is determined by the combination of the evolution of the underlying mass fluctuations, and the bias relating the galaxy overdensities to mass. Observationally the amplitude of the galaxy correlation function has been measured from redshift surveys extending up to redshifts $z\sim 1$ (e.g. CFRS, Le Fevre et al., 1995; CNOC2, Carlberg et al. 1998). The discovery of Lyman Break Galaxies (Steidel et al., 1996) has allowed the scientific community to push this limit even further up to $z\simeq 3$. However there is still a gap between the measurements obtained for $z\lesssim 1$ and those provided by the analysis of the Lyman Break Galaxies at redshifts z=3.

The aim of this letter is to "fill in" this gap by presenting measurements of the correlation function obtained from the catalogue of photometric redshifts derived from the Hubble Deep Field by Fernandez-Soto et al., 1998. Using the photometric redshifts we divide the catalogue into subsamples in redshift and measure the angular correlation function $w(\theta)$ and its amplitude as a function of z up to $z \simeq 4.8$. At low redshift our results agree with the results of Connolly et al. (1998), and at higher redshifts they are consistent with Lyman Break Galaxies.

The outline of the paper is as follows: section 2 gives a description of the catalogue adopted for our analysis while section 3 presents the results for the angular correlation function. In section 4 we derive the meaningful spatial quan-

tities as a function of redshift, while section 5 summarises our conclusions.

2 THE DATA

The Hubble Deep Field (HDF) image (Williams et al., 1996) covers an L-shaped area roughly $3' \times 3'$, with a total area $\sim 4 \mathrm{arcmin}^2$ and provides us with the deepest view of the Universe obtained so far. The image was obtained by the Hubble Space Telescope using the Wide Field Planetary Camera 2 (WFPC2) over a period of 10 consecutive days. The same image was acquired by using the broad-band filters F300W, F450W, F60W and F814W in order to allow for the possibility of assigning photometric redshifts to the objects in the field.

Since then various techniques for getting photometric redshifts have been applied to the HDF (see e.g. Connolly et al., 1998). The catalogue we will use for this work has been derived by Fernandez-Soto et al., 1998 by incorporating in their former technique (Lanzetta et al., 1996) the infrared images of the HDF acquired in the J(1.2 μ m), H(1.65 μ m) and K(2.2 μ m) broad-band filters (Dickinson et al., 1998). Their final catalogue includes 1067 objects, some of them at very high redshifts ($z_{max} \sim 6$), as seen in the redshift distribution shown in Figure 1. The edges of the Wide Field Camera images are of poorer quality than the bulk of the images, and Fernandez-Soto et al. use a magnitude limit of AB(8140)=28 for the inner part of the HDF, while the outer part of the image includes only objects with AB(8140)<26. Using the sensitivity map given in Fernandez-Soto et al.,

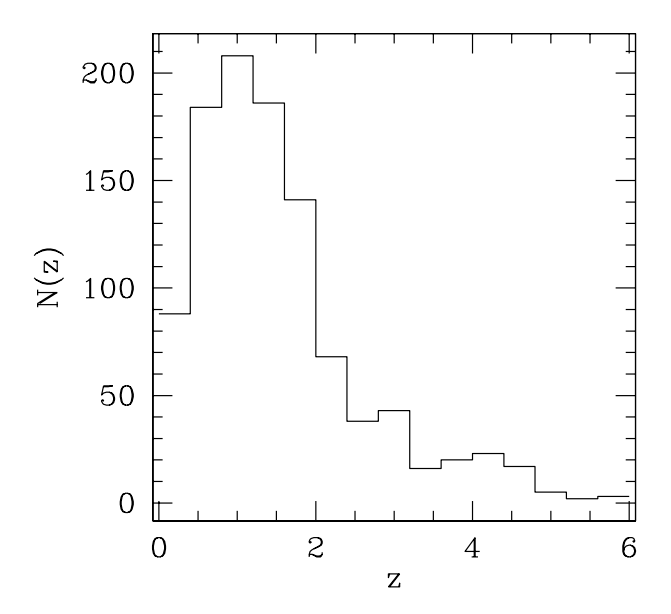


Figure 1. Redshift distribution of the objects in the HDF as obtained by Fernandez-Soto et al., 1998

1998 we rejected all those galaxies belonging to the shallower region; our final version of the catalogue, complete down to the magnitude AB(8140)=28, includes 946 objects. Figure 1 shows the distribution of galaxies in the catalogue split into a series of narrow redshift intervals.

3 THE ANGULAR CORRELATION FUNCTION

Correlation-function analysis has become the standard way to quantify the clustering of different populations of astronomical sources. Ideally we would like to measure the spatial correlation function, but photometric redshifts are not precise enough to enable a direct measurement: the typical error between the photometric estimates and the spectroscopic measurements of z is $\Delta z_{rms} \simeq 0.1 \cdot (1+z)$ $(\Delta z = z_{sp} - z_{phot})$ (see Fernandez-Soto et al., 1998), so that for instance $\Delta z_{rms} \sim 0.4$ at z = 3, corresponding to several hundred Mpc. Nevertheless the estimated redshifts can be used to select subsamples of galaxies at different redshifts, and so we can obtain estimates of the spatial clustering as a function of redshift via the angular correlation function. As pointed out by Connolly at al (1998), the angular correlation function from a redshift limited sample has much higher signal-to-noise than a comparable magnitude limited sample.

The angular two-point correlation function $w(\theta)$ gives the excess probability, with respect to a random Poisson distribution, of finding two sources in the solid angles $\delta\Omega_1$ $\delta\Omega_2$ separated by an angle θ , and it is defined as

$$\delta P = n^2 \delta \Omega_1 \delta \Omega_2 \left[1 + w(\theta) \right] \tag{1}$$

where n is the mean number density of objects in the catalogue under consideration. One of the major limitations on the study of Large-Scale Structure with the HDF is its small field of view; for $\Omega_0 = 1$, 220 arcsecs correspond to

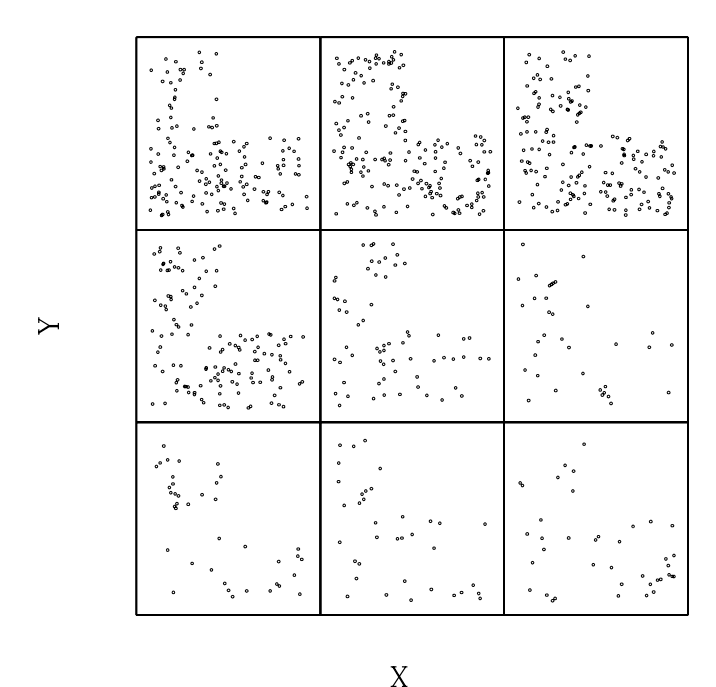


Figure 2. Spatial distribution of objects in the HDF with AB(8140) < 28 in different redshifts intervals: 0.4 - 0.8, 0.8 - 1.2, 1.2 - 1.6, 1.6 - 2.0, 2.0 - 2.4, 2.4 - 2.8, 2.8 - 3.2, 3.2 - 4.0 and 4.0 - 4.8. The resdhift binning is as in Figure 3

 $0.9h^{-1}$ Mpc at z=1, (see Connolly et al., 1998), so isolating narrow redshift intervals will select galaxies in a small volume, and so lead to very large errors in the clustering analysis (e.g. a single cluster of galaxies could dominate the signal). We therefore decided to divide the sample into bins of width $\Delta z = 0.4$ and consider for our analysis all the objects in the "clean" catalogue (see section 2) up to redshifts z = 4.8. This redshift bin width corresponds to between one and two times the expected rms error in the redshifts. Given the small number of galaxies in the catalogue it might be thought that the signal-to-noise could be improved by using broader bins to increase the number of objects per bin and so reduce the Poisson noise. However, increasing the redshift range in each bin would lead to a noticeable reduction of the clustering signal due to the "washing out" of real structures caused by projection effects. As we will see later, cosmic variance is not a problem in our analysis. In fact, the presence of an overdense (underdense) region in the sample would result in a sudden rise (fall) of the clustering amplitude only in one particular redshift bin. The smooth trend of the correlation length r_0 as a function of z (see Figure 4) suggests this is not the case in our analysis.

We then generated random catalogues containing 10000 galaxies, with positions of the random objects lying within the area defined by the geometry of the photometric data, for each of the subsamples associated to a particular redshift bin and then counted the number of distinct data-data pairs (DD), data-random pairs (DR), and distinct random-random pairs (RR) as a function of angular separation. We then calculate w using the estimator (Hamilton, 1993)

$$w = \frac{4DD RR}{DR^2} -1 \tag{2}$$

in the angular scales $9 \le \theta \le 180$ arcsecs. We also used the

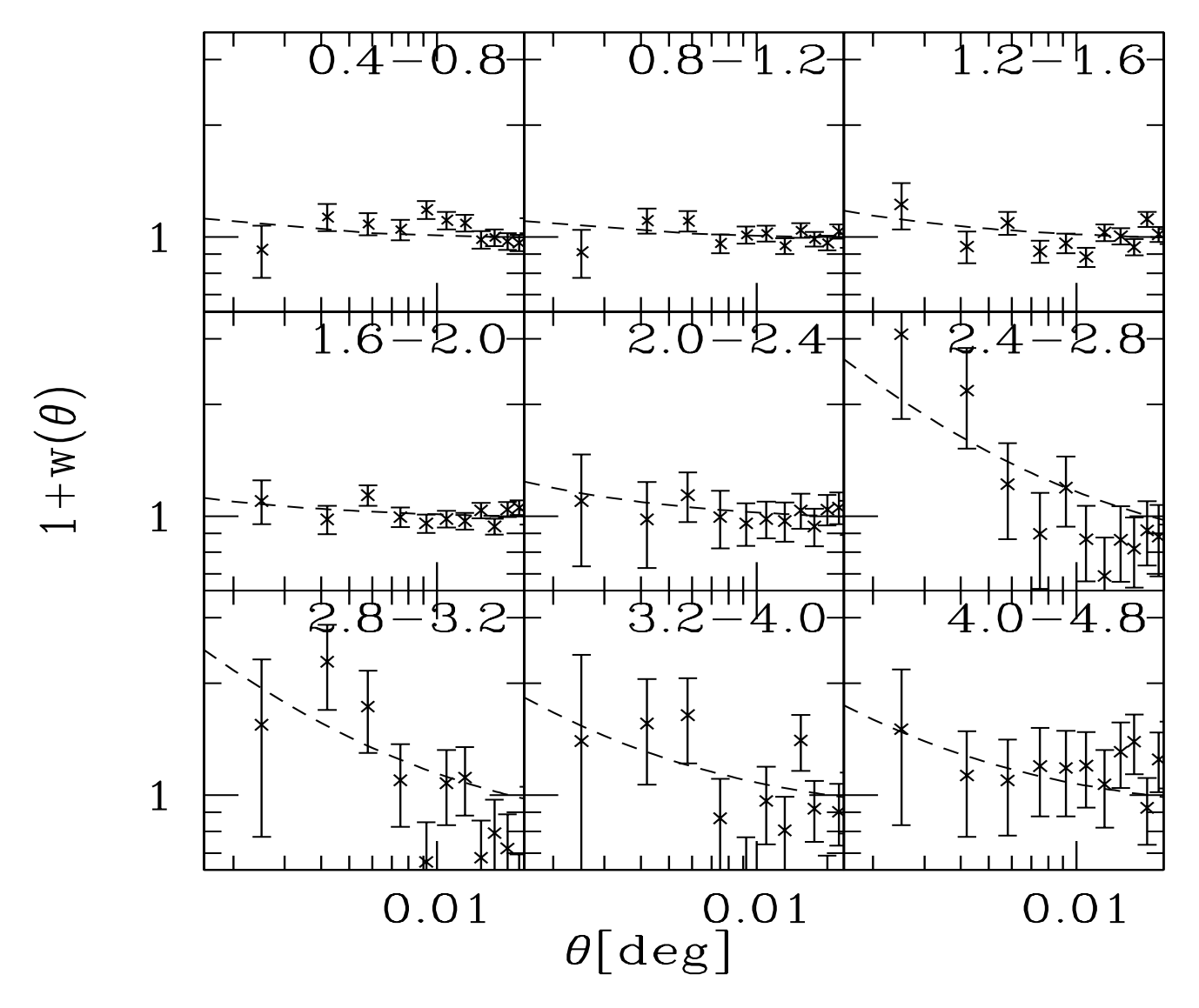


Figure 3. The angular correlation function w for galaxies within the HDF with AB(8140)<28 at different redshifts intervals. The dashed lines show the best fits to the data.

estimators suggested by Peebles (1980) and Landy & Szalay (1993), and found virtually identical results. In Figure 3 we show the results for w for different redshift bins; the error bars show Poisson estimates for the points. Since the distribution is clustered, these estimates only provide a lower limit to the uncertainties. Nevertheless it can be shown that, over the range of scales considered for the calculation of $w(\theta)$, Poisson errors are comparable to those obtained from bootstrap resampling (Villumsen et al., 1997, see also Connolly et al., 1998).

Note that in our analysis we did not include the results for $0 \le z \le 0.4$; this is due to the fact that the effect of excluding bright (nearby) galaxies in the construction of the HDF sample results in a spurious reduction of the clustering amplitude in that redshift range (Connolly et al., 1998).

As shown in Figure 3 the angular correlation function is significantly positive at small scales for all the redshift bins considered in our analysis. The clustering amplitude is roughly constant within the errors up to $z\sim 2.4$; above

this value the amplitude increases, and remains high for all z>2.4 samples.

The apparent clustering in the higher redshift samples may be partly affected by the problem of defining single galaxies from the irregular morphology of some of the objects. However, this is a problem only for scales smaller than 3", and we can see from visual inspection of the distribution of sources in Figure 2 that there are several clumps covering 10-20 arcsec in each sample; it is these that generate the high clustering amplitude. To make sure the signal was not spurious, caused for example by difficulties in identifying single galaxies from complex irregular galaxies, we visually inspected the objects in each of these clumps. The individual galaxies appeared well separated and certainly not parts of single irregular objects. We conclude that the measurements represent real galaxy clustering.

If we assume a power-law form for $w(\theta) = A\theta^{1-\gamma}$, we can estimate the parameters A and γ , using a least-squares fit to the data. Given the large errors on w we assumed a



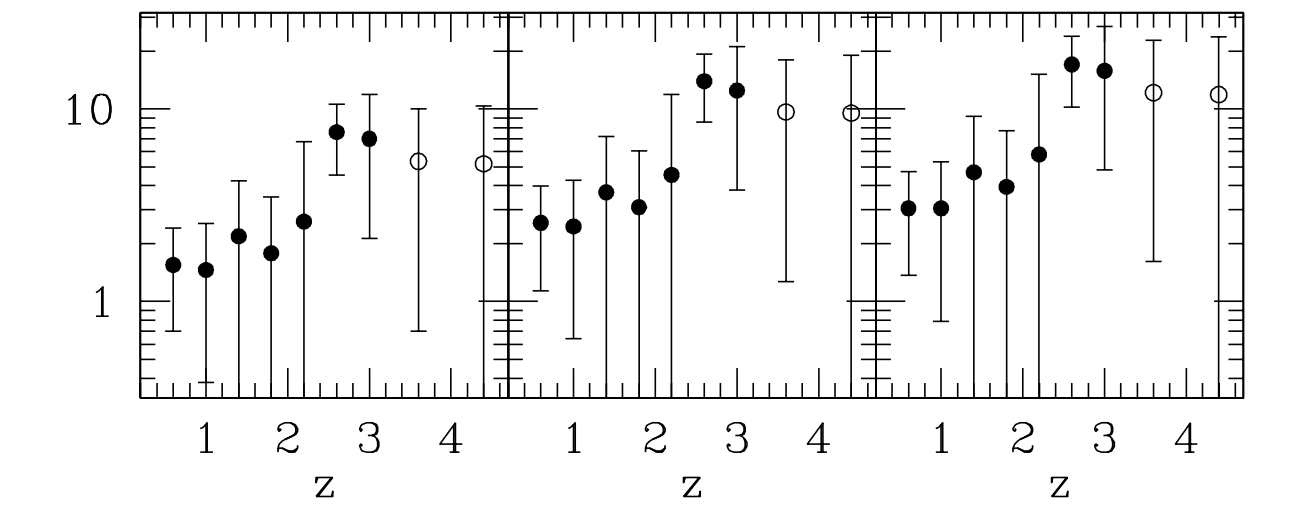


Figure 4. Trend of r_0 as a function of redshift as obtained from the analysis of the HDF photometric redshift catalogue by Fernandez-Soto et al., 1998. The left panel shows results for $\Omega_0=1$, $\Lambda=0$ and $h_0=1$, the panel in the middle shows results for $\Omega_0=0.4$, $\Lambda=0$ and $h_0=0.65$ while the right panel is for $\Omega_0=0.4$, $\Lambda=0.6$ and $h_0=0.65$. The filled points have been derived from considering redshift bins of width $\Delta z=0.4$, while the empty ones are for $\Delta z=0.8$.

fixed value of $\gamma=1.8$. The small area of the HDF catalogue introduces a negative bias through the integral constraint, $\int w^{est} d\Omega = 0$. We allow for this by fitting to $A\theta^{1-\gamma} - C$, where C=25A, Furthermore, even though $w(\theta)$ has been measured up to $\theta \simeq 0^{\circ}.05$, only angular scales less than half the sample size are likely to be reliable (see also Connolly et al., 1998), so we limit the fit to $\theta \simeq 0^{\circ}.02$. The dashed lines in Figure 3 represent the best fit for each redshift interval; the best values for the amplitude A as a function of redshift are listed in Table 1. These values coincide within the errors with the results obtained by Connolly et al. in their analysis of the clustering in the HDF for $z\lesssim 1.4$.

4 RELATION TO SPATIAL QUANTITIES

The standard way of relating the angular two-point correlation function $w(\theta)$ to the spatial two-point correlation function $\xi(r,z)$ is by means of the relativistic Limber equation (Peebles, 1980):

$$w(\theta) = 2 \frac{\int_0^\infty \int_0^\infty F^{-2}(x) x^4 \Phi^2(x) \xi(r, z) dx \, du}{\left[\int_0^\infty F^{-1}(x) x^2 \Phi(x) dx\right]^2},\tag{3}$$

where x is the comoving coordinate, F(x) gives the correction for curvature, and the selection function $\Phi(x)$ satisfies the relation

$$\mathcal{N} = \int_0^\infty \Phi(x) F^{-1}(x) x^2 dx = \frac{1}{\Omega_s} \int_0^\infty N(z) dz, \tag{4}$$

in which \mathcal{N} is the mean surface density on a surface of solid angle Ω_s and N(z) is the number of objects in the given survey within the shell (z, z + dz). Given the small range of angular scales sampled by the HDF we can reasonably as-

sume $\xi(r,z)$ to have the redshift dependent power-law form

$$\xi(r,z) = \left(\frac{r}{r_0(z)}\right)^{-\gamma} \tag{5}$$

where all the dependence on z is included in the correlation scale length $r_0(z)$. The physical separation between two sources separated by an angle θ is given (in the small angle approximation) by:

$$r \simeq \frac{1}{(1+z)} \left(\frac{u^2}{F^2} + x^2 \theta^2\right)^{1/2}.$$
 (6)

By including equations (4), (5) and (6) in equation (3) we then get the following expression for the angular correlation function $w(\theta)$

$$w(\theta) = \frac{H_{\gamma} \int_{0}^{\infty} N(z)^{2} P(\Omega_{0}, z) (x(z) \theta)^{1-\gamma} r_{0}(z)^{\gamma} F(z) dz}{\frac{c}{H_{0}} \left[\int_{0}^{\infty} N(z) dz \right]^{2}}$$
(7)

with $H_{\gamma}=\Gamma[1/2]\Gamma[(\gamma-1)/2]/\Gamma[\gamma/2]=3.68$ in the case of $\gamma=1.8,\ H_0$ the Hubble constant and Ω_0 is the density parameter, and P=dx/dz.

If we consider a narrow redshift bin Δz centred at some \bar{z} we can consider N(z) constant in that interval. Under this assumption the expression for the correlation length $r_0(\bar{z})$ in comoving coordinates is given by:

$$r_0(\bar{z}) = \left(\frac{c A_{\Delta z} \Delta z}{H_0 H_{\gamma} x(\bar{z})^{1-\gamma} P(\Omega_0, \bar{z}) F(\bar{z})}\right)^{1/\gamma}$$
(8)

where $A_{\Delta z}$ is the amplitude of the angular correlation function $w(\theta)$ for a particular redshift interval. Note that in practice the error in redshifts (true Δz) is the convolution of the measured Δz with the error distribution. Assuming Gaussian error distribution, this will increase the effective Δz in

Δz	$ar{z}$	N_{gal}	A	r_0 (a)	r_0 (b)	r_0 (c)
0.4 - 0.8	0.6	151	$(0.7 \pm 0.4) \cdot 10^{-3}$	1.55 ± 0.85	2.56 ± 1.42	3.05 ± 1.68
0.8 - 1.2	1.0	173	$(0.6 \pm 0.4) \cdot 10^{-3}$	1.46 ± 1.08	2.45 ± 1.81	3.05 ± 2.26
1.2 - 1.6	1.4	165	$(1.2 \pm 1.0) \cdot 10^{-3}$	2.18 ± 2.06	3.69 ± 3.52	4.69 ± 4.47
1.6 - 2.0	1.8	161	$(0.8 \pm 0.7) \cdot 10^{-3}$	1.78 ± 1.71	3.09 ± 2.95	3.94 ± 3.77
2.0 - 2.4	2.2	66	$(1.6 \pm 2.3) \cdot 10^{-3}$	2.60 ± 4.18	4.55 ± 7.31	5.80 ± 9.34
2.4 - 2.8	2.6	36	$(11 \pm 4.0) \cdot 10^{-3}$	7.58 ± 3.04	13.9 ± 5.36	17.0 ± 6.83
2.8 - 3.2	3.0	36	$(9.8 \pm 7.0) \cdot 10^{-3}$	7.00 ± 4.87	12.4 ± 8.66	15.8 ± 10.9
3.2 - 4.0	3.6	37	$(5.6 \pm 5.0) \cdot 10^{-3}$	5.35 ± 4.65	9.65 ± 8.38	12.2 ± 10.5
4.0 - 4.8	4.4	39	$(5.9 \pm 5.0) \cdot 10^{-3}$	5.19 ± 5.17	9.52 ± 9.49	11.8 ± 11.8

Table 1. Results for each redshift range, Δz : mean redshift \bar{z} ; number of galaxies; amplitude of the angular correlation function at 1°, A; the spatial clustering amplitude r_0 for three different cosmologies (a) $\Omega_0 = 1$, $\Lambda = 0$, $h_0 = 1$; (b) $\Omega_0 = 0.4$, $\Lambda = 0$, $h_0 = 0.65$; (c) $\Omega_0 = 0.4$, $\Lambda = 0.6$, $h_0 = 0.65$.

equation (8) by a factor $\sqrt{\frac{12\sigma^2}{(\Delta z)^2} + 1}$, where Δz is the bin width and $\sigma = 0.1(z+1)$ is the rms error on each redshift.

The geometry of space will determine the comoving coordinate x, the curvature correction factor F(x) and the quantity $P(\Omega_0, z)$. In particular, for a Universe with generic density parameter Ω_0 and cosmological constant $\Lambda=0$ (see e.g. Magliocchetti et al., 1998; Treyer & Lahav, 1996) we have:

$$x = \frac{2c}{H_0} \left[\frac{\Omega_0 z - (\Omega_0 - 2)(1 - \sqrt{1 + \Omega_0 z})}{\Omega_0^2 (1 + z)} \right], \tag{9}$$

$$F(x) = \left[1 - \left(\frac{H_0 x}{c}\right)^2 (\Omega_0 - 1)\right]^{1/2}$$
 (10)

and

$$P(\Omega_0, z) = \frac{\Omega_0^2 (1+z)^2 (1+\Omega_0 z)^{1/2}}{4(\Omega_0 - 1)[(1+\Omega_0 z)^{1/2} - 1] + \Omega_0^2 (1-z) + 2\Omega_0 z}$$
(11)

In the case of a cosmological constant $\Lambda \neq 0$ with $\Omega_0 + \Lambda = 1$ (flat space) we have F(x) = 1,

$$x = \frac{c}{H_0} \Omega_0^{-1/2} \int_0^z \frac{dz}{\left[(1+z)^3 + \Omega_0^{-1} - 1 \right]^{1/2}},\tag{12}$$

(see Peebles, 1984; Magliocchetti et al., 1998; Treyer & Lahav, 1996) and

$$P(\Omega_0, z) = \Omega_0^{1/2} [(1+z)^3 + \Omega_0^{-1} - 1]^{1/2}.$$
 (13)

Using the values of $A_{\Delta z}$ obtained in section 3, and once again using $\gamma=1.8$ we find the values for the correlation length r_0 listed in Table 1, according to the different cosmologies used in the deprojection analysis. Figure 4 shows the trend of r_0 as a function of the redshift z for the three cosmological models $\Omega_0=1$, $\Lambda=0$, $h_0=1$ (left panel), $\Omega_0=0.4$, $\Lambda=0$, $h_0=0.65$ (central panel) and $\Omega_0=0.4$, $\Lambda=0.6$, $h_0=0.65$ (right panel). Given the uncertainties in the determination of the photometric redshifts at high z's (see section 3), for z<3.2 we have plotted the measurements coming from a $\Delta z=0.4$ binning (filled circles), while for $z\gtrsim3.2$ we only considered broader bins of width $\Delta z=0.8$ (empty circles).

The figure shows that r_0 is roughly constant with look-back time for $z\lesssim 2.4$. Above this redshift, the clustering amplitude increases by more than a factor of 2. Our measurements at high redshifts are in excellent agreement with

the values obtained in the analysis of the clustering of the Lyman Break Galaxies (e.g., for $\Omega_0=1,\,r_0=4\pm1$ - Adelberger et al., 1998 and $r_0=2.1\pm0.5$ - Giavalisco et al., 1998, according to the particular sample used). Given the small volume sampled by the HDF data, the uncertainties are large, and the exact form of the evolution of r_0 is not well determined. The measurements are consistent with a slow decline followed by a smooth rise in amplitude above $z\gtrsim2.4$, as predicted by some galaxy formation models. From our measurements alone we cannot rule out a simple smooth increase of r_0 with z, but compared to local surveys our measurements at $z\sim1$ require a significant drop in the correlation length between z=0 and z=1.

5 CONCLUSIONS

We have calculated the angular correlation function of galaxies in the HDF image as a function of redshift up to $z\simeq 4.8.$ We use the catalogue of photometric redshifts obtained by Fernandez-Soto et al., 1998 to select redshift limited subsamples of width $\Delta z=0.4$, and $\Delta z=0.8$ between $z\simeq 0.4$ and $z\simeq 4.8.$ The results show that, while for $z\lesssim 2.4$ the clustering amplitude is roughly constant, for $z\gtrsim 2.4$ there is a significant increase in amplitude.

Converting the projected clustering amplitude into the correlation length r_0 at different redshifts, we find that $r_0(z)$ is roughly constant as a function of look-back time until $z \simeq 2.4$; at higher redshifts the clustering amplitude rises to much higher values than for lower z's. Our high-redshift measurements are in good agreement with those obtained from the analysis of the Lyman Break Galaxies (Adelberger et al., 1998; Giavalisco et al., 1998).

Under the assumption of linear evolution of mass fluctuations, we would expect a slow decrease in r_0 towards higher redshifts. However, we measure the clustering of galaxies, which are biased tracers of the mass. The bias level is unlikely to be a constant as a function of redshift; any galaxy seen beyond $z \sim 2.4$ has formed stars at an epoch earlier than most galaxies, and so is likely to be biased relative to an "average" galaxy. Also, the HDF galaxy sample is selected on observed frame I band and so different populations of galaxies are selected in the different redshift ranges: at $z \sim 1$ the selection is roughly rest-frame B band, but at higher redshift samples are selected on rest-frame UV flux,

which will preferentially select the galaxies with higher starformation rates.

A further complication is caused by the effects of gravitational lensing. We expect that structure in the foreground mass distribution will introduce an extra component of clustering through the gravitational lensing magnification bias (Villumsen et al 1997). The amplitude of this effect depends on the amplitude of mass fluctuations.

Hence the interpretation of galaxy clustering in the HDF at high redshifts is not at all straightforward. Theoretical models (see for instance Kauffmann et al., 1998; Baugh et al., 1998) predict a trend for the evolution of the clustering signal with look-back time that is similar to what detected in our analysis, but their results are strongly model-dependent. We will present a detailed analysis and comparison to models in a future paper.

ACKNOWLEDGEMENTS MM acknowledges support from the Isaac Newton Scholarship. Jarle Brinchmann is warmly thanked for very helpful and stimulating discussions.

REFERENCES

Adelberger K.L., Steidel C.C., Giavalisco M., Dickinson M., Pettini M., Kellog M., 1998; ApJ, 505, 18
Baugh C.M., Benson A.J., Cole S., Frenk C.S., Lacey C.G.,

1998. astro-ph/9811222

Carlberg, R.G.. Yee, H.K.C., Morris, S.L., Lin, H., Sawicki, M., Wirth, G., Patton, D., Shepherd, C.W., Ellingson, E., Schade, D., Pritchet, C.J., Hartwick, F.D.A., 1998; astro-ph/9805131

Connolly A.J., Szalay A.S., Brummer R.J., 1998; ApJ, 499, L125 Dickinson et al., 1998; in preparation

Fernadez-Soto A., Lanzetta K.M., Yahil A., 1998; astro-ph/9809126

Giavalisco M., Adelberger K.L., Steidel C.C., Dickinson M., Pettini M., Kellog M., 1998; ApJ, 503, 543

Hamilton A.J.S., 1993; ApJ, 417, 19

Kauffmann G., Colberg J.M., Diaferio A., White S.M.D., 1998. astro-ph/9809168.

Landy S.D., Szalay, A.S., 1993;

Lanzetta K.M., Yahil A., Fernandez-Soto A., 1996; Nature, 381, 759

Le Fevre O., Hudon D., Lilly S.J., Crampton D., Hammer F., Tresse L., 1996; ApJ, ApJ 464, 79

Magliocchetti M., Maddox S.J., Lahav O., Wall J.V., 1998; astro-ph/9806342

Mo H.J., Jing Y.P., Borner G., 1992; ApJ, 392, 452

Peebles P.J.E., 1980; The Large-Scale Structure of the Universe, Princeton University Press

Steidel C.C., Giavalisco M., Pettini M., Dickinson M., Adelberger K.L., 1996; ApJ, **462**, L17

Treyer M.A., Lahav O. 1996; MNRAS, 280, 469

Villumsen J.V., Freudling W., Da Costa L.N., 1997; ApJ, $\mathbf{481}$, 578

Williams R.E. et al., 1996; AJ, 112, 1335